

# OBSERVATIONS OF THE WIND FROM THE TRANSITING EXOPLANET HD 209458b <sup>1</sup>

Jeffrey L. Linsky

*JILA, University of Colorado and NIST, 440UCB Boulder, CO 80309-0440*

jlinsky@jilau1.colorado.edu

Hao Yang

*JILA, University of Colorado and NIST, 440UCB Boulder, CO 80309-0440*

haoyang@jilau1.colorado.edu

Kevin France

*CASA, University of Colorado, 593UCB Boulder, CO 80309-0593*

Kevin.France@colorado.edu

Cynthia S. Froning

*CASA, University of Colorado, 593UCB Boulder, CO 80309-0593*

cfroning@casa.colorado.edu

James C. Green

*CASA, University of Colorado, 593UCB Boulder, CO 80309-0593*

James.Green@colorado.edu

John T. Stocke

*CASA, University of Colorado, 593UCB Boulder, CO 80309-0593*

stocke@casa.colorado.edu

Steven N. Osterman

*CASA, University of Colorado, 593UCB Boulder, CO 80309-0593*

steven.osterman@colorado.edu

**ABSTRACT**

Using the new Cosmic Origins Spectrograph (COS) on the *Hubble Space Telescope* (*HST*), we obtained the first moderate resolution, high signal/noise ultraviolet spectra of HD 209458 and its exoplanet HD 209458b during transit, both orbital quadratures, and secondary eclipse. We compare transit spectra with spectra obtained at nontransit phases to identify spectral features due to the planet’s atmosphere and wind. We find decreased flux by  $8 \pm 2\%$  in the C II 1334.5323 Å and 1335.6854 Å lines and in the Si III 1206.500 Å line during transit compared to nontransit times in the velocity interval  $-50$  to  $+50$  km s<sup>-1</sup>. The  $8 \pm 2\%$  obscuration of the star during transit is far larger than the 1.5% obscuration by the exoplanet’s disk. Absorption during transit at velocities between  $-50$  and  $+50$  km s<sup>-1</sup> could be explained by a Roche lobe filled with wind material that is optically thick in the C II and Si III lines or by an extended cometary tail. We identify mass loss from the exoplanet’s atmosphere at speeds near  $42 \pm 4$  km s<sup>-1</sup>, the escape speed predicted from the planet’s mass and radius, with a mass loss rate of  $3.2 \times 10^{11}$  g s<sup>-1</sup>.

*Subject headings:* planets and satellites: atmospheres — planets and satellites: individual (HD 209458b) — planets and satellites: physical evolution — stars: individual (HD 209458) — ultraviolet: stars

**1. INTRODUCTION**

Monitoring of radial velocities and spectra of the G0 V star HD 209458 enabled Mazeh et al. (2000) to derive the orbit, mass, radius, and low density of its transiting planet HD 209458b. Subsequent studies by Henry et al. (2000), Charbonneau et al. (2000), among others, have refined these properties. Table 1 lists the properties of HD 209458 and HD 209458b

---

<sup>1</sup>Based on observations made with the NASA/ESA *Hubble Space Telescope*, obtained from the Data Archive at the Space Telescope Science Institute. STScI is operated by the Association of Universities for Research in Astronomy, Inc., under NASA contract NAS 5-26555. These observations are associated with program #11534.

cited by Knutson et al. (2007). HD 209458b is among the best studied Jupiter-like exoplanets located very close to its host star. As a result of its proximity, HD 209458b receives very strong incident radiation (see estimate in Table 1) and stellar wind flux from its host star.

HD 209458b is the first transiting planet for which atmospheric absorption was observed in the resonance lines of H I, C II, O I, and Na I. Using the low resolution G140L grating of STIS, Vidal-Madjar et al. (2004) detected an absorption depth at midtransit of  $5 \pm 2\%$  for the unresolved Lyman- $\alpha$  line,  $13 \pm 4.5\%$  for the O I 1304 Å multiplet, and  $7.5 \pm 3.5\%$  for the C II 1335 Å multiplet. Using the higher resolution G140M mode of STIS, Vidal-Madjar et al. (2003) had previously found that the Lyman- $\alpha$  line flux was reduced by  $15 \pm 4\%$  near the line core during transit. They argued that significant mass loss must be occurring from the planet on the basis of the large obscuration seen in the Lyman- $\alpha$  line, reduction in the line flux out to nearly  $\pm 100$  km s $^{-1}$  from line center, and somewhat more absorption on the blue side of the emission line than the red side. In a reanalysis of the same data set, Ben-Jaffel (2007) argued that the Lyman- $\alpha$  absorption is less than previously stated and that variability of the stellar Lyman- $\alpha$  flux could explain the transit line profile so that no atmospheric evaporation is required. In a subsequent rebuttal, Vidal-Madjar et al. (2008) identified flaws in both arguments.

Looking back on this controversy, we note that it is difficult to measure the exoplanet’s mass loss rate from the Lyman- $\alpha$  line profile obtained with the G140M grating of STIS given the modest S/N and spectral resolution, the broad interstellar absorption in the core of the line, and the time-varying geocoronal and interplanetary emission in the line core. Also the different radial velocities of the star, interstellar absorption, geocoronal emission, and interplanetary emission must be included in the analysis if one is to infer an accurate mass loss rate by comparing the relative amount of absorption during transit in the positive velocity interval (+50 to +100 km s $^{-1}$ ) with the absorption in the negative velocity interval (–50 to –100 km s $^{-1}$ ). This has not yet been done.

With the objectives of measuring an accurate mass loss rate from the planet and testing different physical models for the mass loss, one needs far better data, which requires a new scientific instrument. One needs higher S/N spectra with higher spectral resolution and sufficient sensitivity to study many spectral lines formed in the extended atmosphere and wind of the exoplanet. As we describe below, the new Cosmic Origins Spectrograph (COS) on *HST* is well designed for this task.

## 2. OBSERVATIONS AND DATA REDUCTION

We observed HD 209458 using COS, which was placed on the *HST* during Servicing Mission 4 in 2009 May. COS is a high-throughput ultraviolet (UV) spectrograph optimized for point sources. Descriptions of the on-orbit performance characteristics of COS will be presented by J. C. Green et al. (in preparation) and S.N. Osterman et al. (in preparation). During COS program 11534, we observed HD 209458 with both the G130M and G160M gratings of the far-UV channel to obtain moderate resolution spectra covering the 1140–1790 Å spectral region. In this paper we analyze the spectra obtained with the G130M grating, which includes the spectral range 1140–1450 Å. The G160M observations are presented by France et al. (2010). The COS line spread function in the far-UV is not a simple Gaussian, but it can be approximated by a Gaussian with a resolution of 17,000-18,000 (16.7-17.6 km s<sup>-1</sup>) with extended wings (Ghavamian et al. 2010). Since the emission lines analyzed in this program are broad, the extended wings of the LSF do not significantly affect our results.

Table 2 summarizes the individual G130M exposures obtained at transit (near orbital phase 0.00), first quadrature (phase 0.25), secondary eclipse (phase 0.50), and second quadrature (phase 0.75). The total exposure times for these phases are 4946.8 s, 7941.7 s, 4956.7 s, and 7796.0 s, respectively. The orbital phases listed in Table 2 are computed using the ephemeris of Knutson et al. (2007). Transit occurs between orbital phases 0.982 and 0.018 (Wittenmyer et al. 2005) as indicated by the optical light curve. The duration of transit is about 3.22 hours. *HST* was therefore able to observe HD 209458 during transit on two sequential spacecraft orbits.

The signal/noise in COS spectra is lower than predicted by photon statistics as a result of two instrumental effects. The hex pattern formed at the intersection of the microchannel plate pores imposes a  $\pm 4\%$  pattern on the spectral signal, and shadows of the wire grid on the detector decreases the signal as much as 20% at certain locations on the detector faceplate. We checked the locations of the known wire grid shadows and found that the spectra of the C II, Si III and Si IV lines studied in this paper are not affected by the wire grids. Both effects, which are fixed at the detector, were mitigated by moving the grating and the resultant spectrum to different positions on the detector. In this program we observed at four different grating positions identified by the beginning and ending wavelengths of the gap between the two detector faceplate elements listed in the last column of Table 2. In principle, division of a transit spectrum by a nontransit spectrum at the same grating position should cancel the signal errors introduced by both instrumental effects to show the true spectral difference produced by the planet in front of the star. In practice, the cancellation will not be perfect because of possible time variations in the stellar spectrum, positioning errors of the star in the aperture, and grating mechanisms that do not come to the same position

every time. These errors will change the location of a spectral element on the detector. Also, within 500 pixels of the end of each detector segment (about 5 Å for G130M) there are additional instrumental artifacts in the spectrum. For these reasons, we compare only transit and nontransit spectra obtained at the same grating settings, and do not analyze portions of the spectrum near the ends of a detector faceplate. The data were processed with the COS calibration pipeline, CALCOS<sup>2</sup> v2.11b (2009-09-08), combined with a custom IDL coaddition procedure.

Figure 1 shows a portion of the G130M spectrum obtained during all transit and all non-transit observations (secondary eclipse and both quadratures). The spectra are very similar, but there are subtle differences that provide information on the exoplanet and its atmosphere. In this paper we compare transit and nontransit spectra of lines of C II, Si III, and Si IV. The H I Lyman- $\alpha$  line cannot be analyzed because geocoronal emission through the large aperture of COS completely dominates any stellar component. The O I lines at 1302, 1304, and 1306 Å were also not analyzed because time-varying geocoronal emission in these lines renders comparison of transit and nontransit spectra uncertain and because the lines were located close to the end of a detector faceplate.

### 3. RESULTS

#### 3.1. Si IV Line

A critical question is whether the emission line fluxes of the host star were significantly different at the times when the transit and nontransit spectra were obtained, since late-type stars like the Sun often show time-variable emission in lines formed in their outer atmospheres (e.g., Rottman 2006). Figure 2 shows the coadded transit and nontransit spectra for the Si IV resonance line (1393.76 Å). Since the Si IV line is formed in highly ionized gas that is not likely to be in the atmosphere or extended wind of the exoplanet, the very similar Si IV fluxes during times of transit and nontransit indicate that the average flux in the stellar emission lines during our observations was nearly constant. We find that the average transit/nontransit flux ratio for the velocity range between  $-50$  and  $+50$  km s<sup>-1</sup> was  $0.998 \pm 0.021$ . We therefore assume that the mean stellar flux in the other emission lines was the same during transit and nontransit times and do not rescale the transit and nontransit fluxes.

---

<sup>2</sup>We refer the reader to the cycle 18 COS Instrument Handbook for more details: [http://www.stsci.edu/hst/cos/documents/handbooks/current/cos\\_cover.html](http://www.stsci.edu/hst/cos/documents/handbooks/current/cos_cover.html).

### 3.2. C II Lines

The C II lines at 1334.5323 Å and 1335.6854 Å are bright emission lines formed in the chromospheres of solar-type stars like HD 209458. On October 02, 2009, we observed the C II lines during transit with the G130M grating at four grating positions specified by the gap wavelengths listed in Table 2. For each of these grating positions there are corresponding observations at both quadratures and a secondary eclipse obtained at different times.

Figure 3 shows the coadded spectra of the C II 1334.5323 Å resonance line and the C II 1335.6854 Å line. The spectra were smoothed with a 5 pixel boxcar. The on-orbit G130M spectral resolution element is 7–8 pixels. The transit and nontransit spectra are plotted separately and ratioed. The deep minimum observed in the C II 1334.5323 Å line at  $-6.60$  km s $^{-1}$  (heliocentric) is interstellar absorption due to the Eri cloud located within 3.5 pc of the Sun (Redfield & Linsky 2008). Since the radial velocity of HD 209458 is  $-14.8$  km s $^{-1}$ , the interstellar absorption is centered to the red of the centroid of the stellar emission line.

Both C II lines show less flux during transit than nontransit times, although the error bars for some velocity pixels overlap. We plot the transit/nontransit flux ratios between  $-50$  and  $+50$  km s $^{-1}$ . Further out in the line wings, the fluxes are too small for meaningful ratios. The C II 1334.5323 Å line ratio is generally less than 1.0 between  $-50$  and  $+20$  km s $^{-1}$  and beyond  $+30$  km s $^{-1}$ . The C II 1335.6854 Å line ratio is less than 1.0 between  $-50$  and  $0$  km s $^{-1}$  and then beyond  $+10$  km s $^{-1}$ . The mean transit/nontransit flux ratio in the velocity interval  $-50$  to  $+50$  km s $^{-1}$  is  $0.924 \pm 0.022$  for the C II 1334.5323 Å line and  $0.921 \pm 0.015$  for the C II 1335.6854 Å line.

### 3.3. Si III Line

Figure 2 shows the coadded transit and nontransit spectra for the Si III resonance line at 1206.500 Å. The mean transit/nontransit flux ratio for the Si III line in the velocity interval  $-50$  to  $+50$  km s $^{-1}$  is  $0.918 \pm 0.014$ .

## 4. DISCUSSION

The  $8 \pm 2\%$  obscuration of the star in the C II and Si III lines during transit far exceeds the 1.5% obscuration by the exoplanet’s disk, indicating absorption by an extended atmosphere or wind that is optically thick in the C II and Si III lines. Our result for the C II lines is consistent with the value of  $7.5_{-3.4}^{+3.6}$  fractional absorption depth that Vidal-Madjar

et al. (2004) obtained for the unresolved C II lines, but inconsistent with the fractional absorption depth of  $0.0_{-0.0}^{+2.2}$  that they obtained for the Si III lines. Their fractional absorption depth of  $0.0_{-0.0}^{+6.5}$  of the Si IV line is consistent with our value.

We note that the velocity interval in which this absorption is detected (up to  $50 \text{ km s}^{-1}$  towards the observer) is similar to the escape speed ( $42 \text{ km s}^{-1}$ ) of a wind from HD 209458b computed from the mass and radius of the planet (Table 1). Since the size of the obscuring material (if optically thick in these lines) is similar to the size of the exoplanet’s Roche lobe, one possible explanation for the transit data is that the Roche lobe is filled by gas from the wind. Another possible explanation is that the exoplanet’s wind forms an extended cometary tail blown out by the stellar wind, as suggested by hydrodynamical simulations (Schneider et al. 2007).

We estimate the mass loss rate from the planet’s atmosphere assuming that the outflow forms a spherically symmetric envelope around the planet that is optically thick in the C II resonance line covering about 8% of the stellar surface. The envelope becomes optically thin at its “limb” because the expansion of the wind in three dimensions and conservation of mass flux reduces the gas density with increasing radial distance ( $r$ ) from the planet. We define the envelope “limb” to be at the radial distance from the planet for which the absorption area is the same as that of an opaque sphere of the same size.

We consider a line of sight from the star that passes through the envelope with  $p$  the point of closest approach to the planet. The quantity  $x$  measures the distance along this line of sight from point  $p$  back to the star. The optical depth in the C II resonance line along this line of sight at the apparent limb of the envelope is,

$$\tau[p(\Delta\nu)] = 2k \int_0^\infty n_{C II}(x) dx = 0.69, \quad (1)$$

where  $n_{C II}$  is the number density of  $C^+$  ions,  $k = \frac{\sqrt{\pi}e^2}{mc} \frac{f}{\Delta\nu_D}$  is the line opacity,  $f = 0.128$  is the oscillator strength,  $m$  is the electron mass, and  $\Delta\nu_D$  is the Doppler parameter. The value of  $p$  depends somewhat on the displacement from line center,  $\Delta\nu$ , because for an expanding wind, most of the absorption occurs near the frequency corresponding to the line of sight component of the expansion velocity. The “limb” occurs at  $\tau = 0.69$ , where as much stellar flux is transmitted through the envelope for lines of sight passing inside of  $p$  than for those passing outside of  $p$ ,  $\int_{0.69}^\infty e^{-t} dt = \int_0^{0.69} e^{-t} dt$ , where  $t$  is the optical depth for lines of sight with different values of  $p$ .

Since the gas density decreases with increasing  $r$  and thus increasing  $x$  along the line of sight,  $p(\Delta\nu)$  should increase slightly with increasing  $\Delta\nu$ . We compute  $\Delta\nu_D = 2.7 \times 10^{10} \text{ s}^{-1}$ ,

assuming a gas temperature of 10,000 K (Garcia Muñoz 2007). If the outflow is turbulent, then  $\Delta\nu_D$  will be larger. For spherical outflow at constant escape speed ( $v_{esc} = 4 \times 10^6$  cm s<sup>-1</sup>), the mass flux of C<sup>+</sup> ions from the planet is

$$\dot{M}_{C II} = 4\pi r^2 m_C v_{esc} n_{C II}(r), \quad (2)$$

where  $n_{C II}(r)$  is the number density of C II ions at a radial distance  $r$  from the star,  $m_C$  is the mass of a carbon atom, and  $r^2 = x^2 + p^2$ .

We estimate  $\dot{M}_{C II}$  by requiring that the gas in the wind obscure 8% of the stellar disk at  $\pm 50$  km s<sup>-1</sup> from line center. This will occur when the optical depth at this velocity is about 0.3 at  $p^2 = 0.08 R_\star^2$ , i.e.,

$$\tau(p = 0.284 R_\star) = \frac{2\sqrt{\pi} e^2 f \dot{M}_{C II}}{m_C \Delta\nu_D 4\pi m_C v_{esc}} \int_0^\infty \frac{dx}{r^2} = 0.69. \quad (3)$$

The integral has an analytical solution by setting  $u = x/p$ ,

$$\int_0^\infty \frac{dx}{r^2} = \frac{1}{p} \int_0^\infty \frac{du}{u^2 + 1} = \frac{\pi}{2p}. \quad (4)$$

We find that

$$\dot{M}_{C II} = 8.5 \times 10^7 \text{ g s}^{-1} = 2.7 \times 10^{15} \text{ g yr}^{-1}. \quad (5)$$

In his model for the wind of HD 209458b, Garcia Muñoz (2007) found that essentially all of the carbon is singly ionized. For a carbon abundance of  $2.7 \times 10^{-4}$  that of hydrogen (Asplund et al. 2009), the total mass loss rate from the planet is,

$$\dot{M}_{total} = 3.2 \times 10^{11} \text{ g s}^{-1} = 9.7 \times 10^{18} \text{ g yr}^{-1}. \quad (6)$$

Several authors (e.g., Ben-Jaffel & Sona Hosseini 2010; Murray-Clay et al. 2009) have developed models for the wind of HD 209458b. From the shape of the absorption during transit of the Lyman- $\alpha$  line, Vidal-Madjar et al. (2003) estimated a minimum mass loss rate of  $10^{10}$  g s<sup>-1</sup>, although we have noted the problems with analyzing this data set. Garcia Muñoz (2007) developed a detailed model for the supersonic velocity wind from HD 209458b by solving the equations of mass, momentum, and energy conservation including tidal forces. He found a mass loss rate of  $6.10 \times 10^{10}$  g s<sup>-1</sup> assuming that the irradiation from the host star

is similar to the Sun at low activity and  $1.52 \times 10^{11} \text{ g s}^{-1}$  for the Sun at high activity. Our value of  $\dot{M}_{total} = 3.2 \times 10^{11} \text{ g s}^{-1}$  (assuming only thermal Doppler broadening) or perhaps larger if turbulent broadening is important, is somewhat larger than that predicted by the Garcia Muñoz (2007) model.

Since the planet’s mass is  $1.2 \times 10^{30} \text{ g}$  (Knutson et al. 2007), the fractional mass loss rate per year is very small,

$$\frac{\dot{M}_{total}}{M_{planet}} = 8.1 \times 10^{-12} \text{ yr}^{-1}. \quad (7)$$

This calculation assumes that the mass loss rate and planetary orbit do not change with time.

## 5. CONCLUSIONS

The high sensitivity and moderate spectral resolution of COS allowed for the first time measurements of gas absorption by the atmosphere and wind of a transiting exoplanet in lines of C II and Si III with velocity resolution. During the transit by HD 209458b, we found that the flux in these lines is reduced by  $8 \pm 2\%$  in the velocity range  $-50$  to  $+50 \text{ km s}^{-1}$ . We find evidence for wind expansion near the escape velocity from the exoplanet with a mass loss rate of  $3.2 \times 10^{11} \text{ g s}^{-1}$ . This is several times larger than predicted by the models of Garcia Muñoz (2007) and in the middle of the range predicted by the models of Murray-Clay et al. (2009) for pre-main-sequence and main-sequence host stars.

This work is supported by NASA through grants NNX08AC146 and NAS5-98043 to the University of Colorado at Boulder. We thank the many people at the Space Telescope Science Institute, Goddard Space Flight Center, Ball Aerospace and Technologies Corp. and CASA at the University of Colorado for the excellent hardware and software that has made COS a great success.

## REFERENCES

- Asplund, M., Grevesse, N., Sauval, J., & Scott, P. 2009, *ARA&A*, 47, 481
- Ben-Jaffel, L. 2007, *ApJ*, 671, L61
- Ben-Jaffel, L. & Sona Hosseini, S. 2010, *ApJ*, 709, 1284

- Charbonneau, D., Brown, T. M., Latham, D., & Mayor, M. 2000, *ApJ*, 529, L45
- Garcia Muñoz, A. 2007, *Planet. Space Sci.*, 55, 1426
- France, K., Stocke, J. T., Yang, H., Linsky, J. L., Froning, C. S., Green, J. C., and Osterman, S. N. 2010, *ApJ*, submitted
- Ghavamian, P. et al. 2010 *BAAS*, 42, 499
- Henry, G. W., Marcy, G. W., Butler, R. P., & Vogt, S. S. 2000, *ApJ*, 529, L41
- Knutson, H. A., Charbonneau, D., Noyes, R. W., Brown, T.M., & Gilliland, R. L. 2007, *ApJ*, 655, 564
- Mazeh, T. et al. 2000, *ApJ*, 532, L55
- Murray-Clay, R. A., Chiang, E. I., & Murray, N. 2009, *ApJ*, 693, 23
- Redfield, S. & Linsky, J. L. 2008, *ApJ*, 673, 283
- Rottman, G. 2006, *Space Sci. Rev.*, 125, 39
- Schneider, E. M., Velázquez, P. F., Esquivel, A., Raga, A. C., & Blanco-Cano, X. 2007 *ApJ*, 671, 57
- Wittenmyer, R. A. et al. 2005, *ApJ*, 632, 1157
- Vidal-Madjar, A. et al. 2003, *Nature*, 422, 143
- Vidal-Madjar, A. et al. 2004, *ApJ*, 604, L69
- Vidal-Madjar, A., Lecavelier des Etangs, A., Désert, J.-M., Ballester, G. E., Ferlet, R., Hébrard, G., & Mayor, M. 2008, *ApJ*, 676, L57

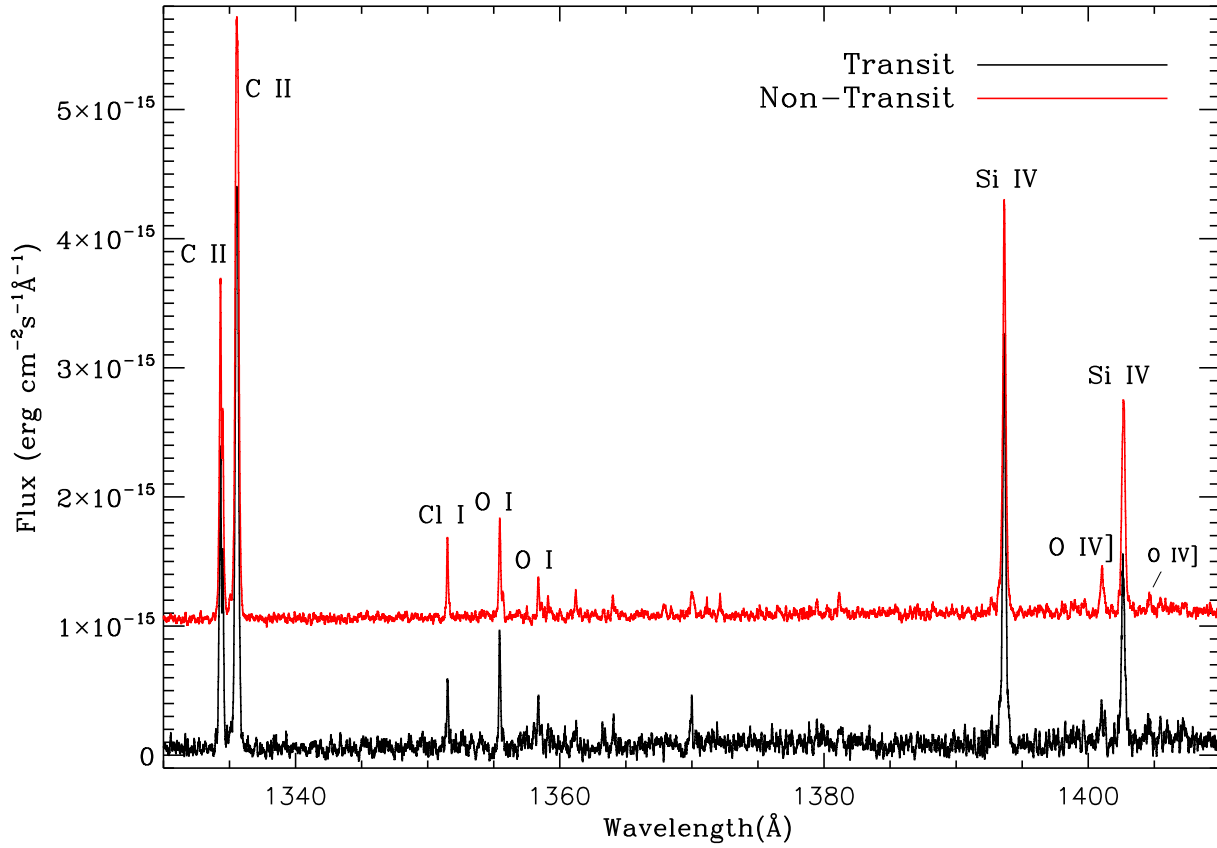


Fig. 1.— A portion of the COS G130M spectrum of HD 209458. The lower (black) plot is the sum of four spectra obtained during transit. The upper (red) plot (displaced upward) is the sum of the ten quadrature and four secondary eclipse spectra.

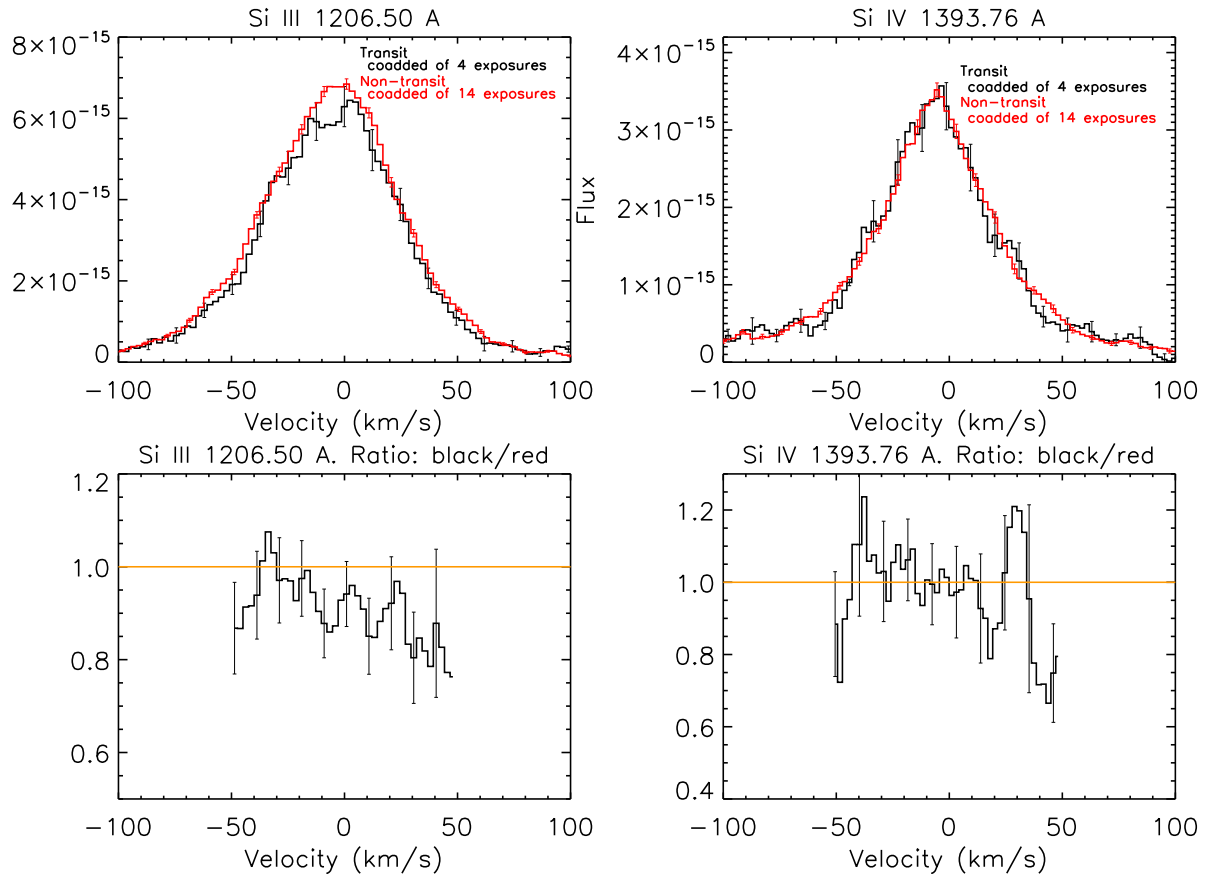


Fig. 2.— Upper panels: Comparison of the four coadded spectra obtained during transit (black) with the coadded nontransit spectra (red). Representative error bars per pixel are included. Lower panels: flux ratios of the transit/nontransit spectra in velocity space. The velocity scale is heliocentric.

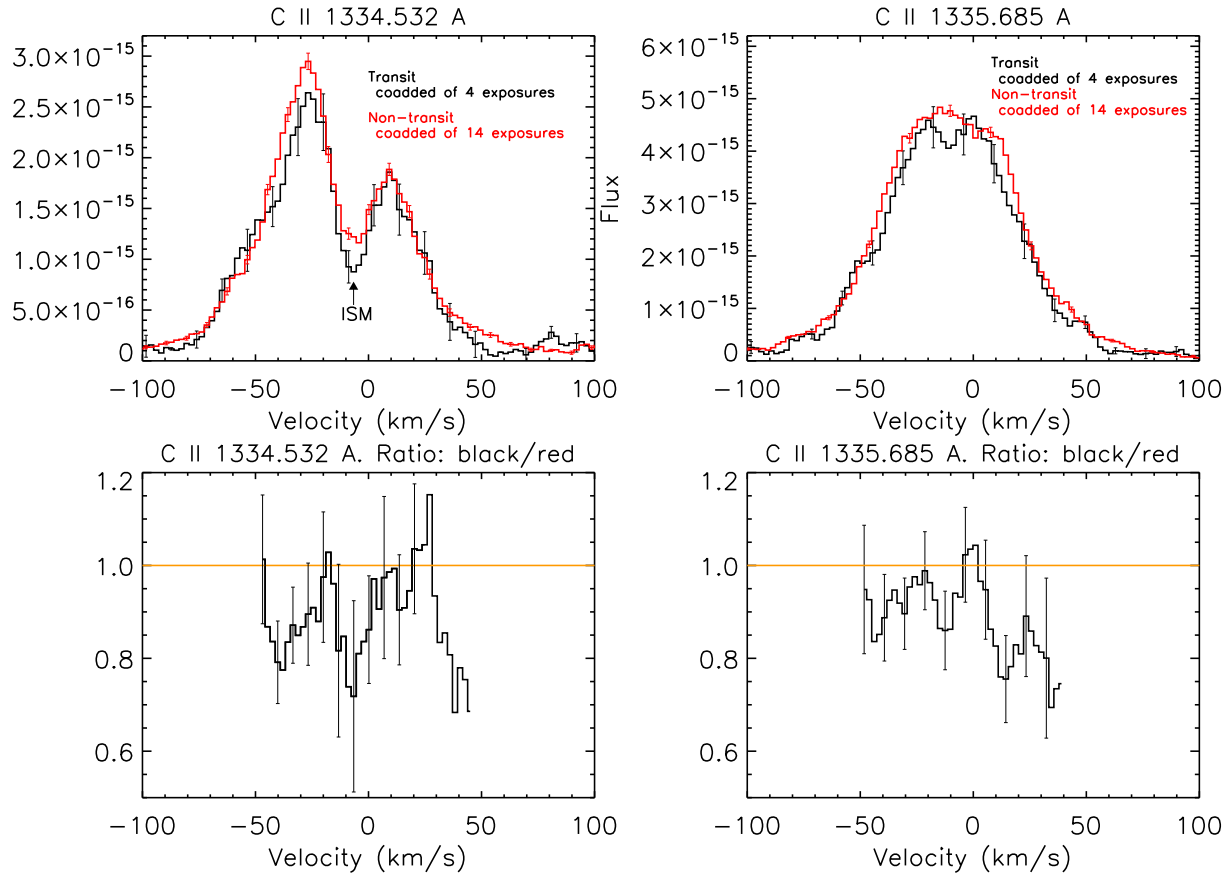


Fig. 3.— Same as Figure 2 except for the C II lines.

Table 1. Properties<sup>a</sup> of HD 209458 and HD 209458b

Spectral type	G0 V
Distance (pc)	47
$M_{\star}/M_{\odot}$	$1.101^{+0.066}_{-0.062}$
$R_{\star}/R_{\odot}$	$1.125^{+0.020}_{-0.023}$
$P_{\text{orbit}}$ (days)	3.52474859(38)
$R_{\text{planet}}/R_{\text{Jup}}$	$1.320^{+0.024}_{-0.025}$
$M_{\text{planet}}/M_{\text{Jup}}$	$0.64 \pm 0.06$
$\rho_{\text{planet}}/\rho_{\text{Jup}}$	$0.26 \pm 0.04$
Semimajor axis (AU)	0.045
Stellar flux at planet/Jupiter	13,400
Escape speed (km/s)	$42 \pm 4$
Orbital Velocity ampl. (km/s)	146
Transit duration (hr)	3.22
Transit depth for $R_{\text{planet}}$	1.5%
Transit depth for $R_{\text{Roche}}$	10%

<sup>a</sup>Data from Knutson et al. (2007).

Table 2. COS E130M Observations of HD 209458 (Program 11534)

Exp. Time (s)	Phase	Day	Start	Stop	Gap <sup>a</sup> (Å)
2340.2	0.2516–0.2593	19 Sep	10:10:15	10:49:15	1278–1290
0955.2	0.2684–0.2716	19 Sep	11:35:37	11:51:32	1288–1299
1851.2	0.2722–0.2782	19 Sep	11:54:40	12:25:31	1296–1306
0560.0	0.2873–0.2891	19 Sep	13:11:29	13:20:49	1288–1299
2235.1	0.2898–0.2971	19 Sep	13:24:06	14:01:21	1306–1316
2340.2	0.7059–0.7136	24 Sep	13:12:09	13:51:09	1278–1290
0945.2	0.7229–0.7260	24 Sep	14:38:04	14:53:49	1288–1299
1787.2	0.7266–0.7324	24 Sep	14:56:57	15:26:44	1296–1306
0925.2	0.7417–0.7448	24 Sep	16:13:54	16:29:19	1288–1299
1798.2	0.7454–0.7513	24 Sep	16:32:36	17:02:34	1306–1316
1045.2	0.9913–0.9947	02 Oct	14:32:10	14:49:35	1278–1290
1096.2	0.9954–0.9990	02 Oct	14:52:52	15:11:08	1288–1299
1400.2	0.0077–0.0123	02 Oct	15:55:28	16:18:48	1296–1306
1405.2	0.0129–0.0175	02 Oct	16:21:56	16:45:21	1306–1316
1057.2	0.4880–0.4915	18 Oct	10:57:04	11:14:41	1278–1290
1093.1	0.4921–0.4957	18 Oct	11:17:49	11:36:02	1288–1299
1401.2	0.5043–0.5089	18 Oct	12:19:37	12:42:58	1296–1306
1405.2	0.5095–0.5141	18 Oct	12:46:06	13:09:31	1306–1316

<sup>a</sup>The gap is the wavelength interval between the two detector faceplate elements. No data are available for the gap region, and there are instrumental artifacts at wavelengths close to the gap.